Identification and Robust Control of the Nonlinear Photoelectrothermal Dynamics of LED Systems

Dong, Jianfei; Zhang, Guoqi

DOI
10.1109/TIE.2016.2619659

Publication date
2017

Document Version
Accepted author manuscript

Published in
IEEE Transactions on Industrial Electronics

Identification and Robust Control of the Nonlinear Photoelectrothermal Dynamics of LED Systems

Jianfei Dong and Guoqi Zhang, *Fellow Member*, *IEEE*

***Abstract*—In lighting systems consisting light emitting diodes (LEDs), excessive temperature is a main cause of degraded luminous efficacy, which leads to reduced average illuminance and distorted illumination rendering. Modeling the thermal dynamics of LEDs is hence essential in designing thermal dissipators and controllers for maintaining constant illuminance or chromaticity. In the existing literature, both physical modeling and system identification have been proposed, which all find the dependence of the temperature on the input power. When the power fluctuates, e.g. due to dimming control, the thermal dynamics becomes nonlinear. Moreover, when a photoelectrothermal (PET) model is used in control synthesis, the nonlinearity due to the product of the temperature dependent efficacy and the input power must be considered. These nonlinearities are either ignored or linearized in most existing methods. The main contribution of this work is treating the aforementioned nonlinearities in a linear parameter varying (LPV) framework. First, the nonlinear thermal dynamics is identified by LPV system identification techniques. Then, a controller to track reference illuminance is designed by $\mathcal{H}_\infty$ control techniques to be robust to both the temperature and the disturbance from ambient light. The identification data and the designed controller are collected from and verified on real experimental setup.**

***Index Terms*—Light emitting diodes (LEDs), photoelectrothermal (PET) dynamics, nonlinear systems, linear parameter varying (LPV), system identification, $\mathcal{H}_\infty$ control.**

I. Introduction

LIGHTING systems based on light emitting diodes (LEDs) have several advantages over conventional light sources like higher efficiency and controllable emission properties [1], and hence hold the promise of providing energy-efficient dynamic and interactive artificial illumination.

The controllable emission properties of LEDs can be attributed to their high switching frequency in the order of mega Hertz. By switching the LEDs on and off with a controlled duty cycle, the luminous flux can be regulated. To enable accurate dimming control, many literatures have been devoted to driver design methods, e.g. [2]–[6]. On the other hand, assuming perfect dimming control, light distribution models have been studied, e.g. in terms of spatial distribution [7] and color rendering [8]. The methods to control the light distribution are developed in [9]–[12] to generate desired spatial illumination patterns and at the same time, improving the energy efficiency. Besides, control methods have also been developed in [13] to maintain the color stability of LED lamps.

Another property of LEDs is that their luminous efficacy gradually decreases as the temperature at their p-n junctions rises [14]. Besides, thermal cycling may cause solder interconnection fatigue damage in LED light sources [15]. Therefore, the recent research has been directed to model the thermal dynamics of LEDs, and to analyse their changed optical properties due to temperature changes. For instance, LED thermal models have been used in analysing the thermal resistance and optical power loss in [16], in predicting the correlated color temperature (CCT) and color rendering index of phosphor-coated white LEDs in [17], and in reducing color variation of white LEDs in [18].

In practice, thermal compensation is usually based on a lookup table of the relationship between the junction temperature and the luminous efficacy. However, this lookup table is usually calibrated at some thermal equilibrium states, and cannot capture the transient dynamic response of the LEDs.

Modeling the thermal dynamics by system identification techniques has been proposed in [19]–[21]. The thermal model is parameterized as a first-order transfer function, and identified at a set of different input power levels. The zeros, poles and gains of the transfer functions are all different among the different conditions. This indicates that the transfer function is not time invariant, but instead depends on the input power. The identified zeros, poles and gains at different input power levels are averaged in [20], resulting in a linear time invariant (LTI) model. The averaged LTI model cannot describe the power dependence of the LED thermal dynamics, especially when the parameters largely vary in the operating range of the power. Therefore, in [21], the possible variation of the parameters from the averaged LTI model is taken into account in the controller design in terms of model uncertainties by means of robust control techniques.

Instead of averaging, the parameters under different operating conditions can be interpolated, and described by a polynomial function of the operating conditions. This is known as interpolation based system identification of linear parameter

Manuscript received March 21, 2016; revised June 6, 2016 and July 31, 2016; accepted August 23, 2016.

J. Dong is with Suzhou Institute of Biomedical Engineering and Technology, Chinese Academy of Sciences, and is also with Beijing Research Center, Delft University of Technology (corresponding author, e-mail: jfeidong@hotmail.com).

G. Zhang is with Delft University of Technology, Delft, the Netherlands, and is also with the Institute of Semiconductors, Chinese Academy of Sciences, and the State Key Laboratory of Solid State Lighting, China (e-mail: g.q.zhang@tudelft.nl).

varying (LPV) systems [22]–[26]. In lighting applications, the input power usually do not change abruptly, but instead in a stepwise fashion. Besides, the LED temperature also changes smoothly when the input power changes. Therefore, the interpolation based LPV identification approach is suitable for identifying the thermal dynamics of LEDs.

In terms of controlling LED lighting systems, one track of research is by feed forward control, e.g. in [9]–[11]. Another track is by feedback control, e.g. PID type of control laws in [19], [27], using loop shaping techniques based on linear LED models. Optimal control methods have also been applied to control LEDs. In [21], the robust control methods are developed to deal with the uncertainties in the PET model. In [28], LQG control method is applied with an observer to estimate the disturbance due to temperature. However, these work has not addressed two issues in controlling the PET dynamics of LEDs. First, the product of the temperature dependent efficacy with the input power results in another form of nonlinearity. This nonlinearity is either ignored or linearized in the methods aforementioned. It is considered in [29], where a nonlinear model predictive control scheme is developed. This method, however, requires solving a nonlinear programming problem online, which is demanding for the microcontrollers (MCUs) commonly used in LED lamps. Second, the disturbance of the ambient light, i.e. the light from other artificial or natural light sources that is not controllable, to the illumination distribution is not considered. This work aims at solving the nonlinearity and robustness issues in the control problem, and deriving a controller that is easy to implement on a low-end MCU.

In this paper, we will investigate the system identification and robust control methods in a unified LPV framework for the nonlinear PET dynamics of LED systems. The rest of the paper is organized as follows. In Sec. II, we describe the nonlinear PET dynamics, and formulate the identification and control problem to be investigated. The nonlinear thermal dynamics is identified by interpolation based LPV identification techniques in Sec. III. The robust control design method is proposed and tested in Sec. IV. Sec. V concludes the paper.

II. Nonlinear photoelectrothermal dynamics

A. Description of the nonlinear dynamics

The temperature of LEDs is determined by the input power to the LED devices. In [20], [21], [30], the dynamic temperature model of LEDs is parameterized as a first order transfer function. In [20], [21], this transfer function is identified at a set of different input power levels. Its zero, pole and gain are all different among the different conditions, indicating the dynamics is not time invariant, but depends on the input power.

In industrial applications, LED lamps are powered by either constant voltage or constant current drivers. The input power is usually not directly controlled. In dimming control, the power is regulated by controlling the duty cycles of pulse width modulated (PWM) current signals, with constant amplitude. Since the natural frequency of LEDs is usually in the magnitude of mega Hz and much higher than the fundamental frequency of the PWM dimming signals (usually a few kilo Hz), the transient response of the luminous flux to the PWM signals can be ignored [31]. The flux emitted by an LED in one period of the PWM signal is hence proportional to the average current flowing through it [9], [32], which equals the product of the duty cycle and the current amplitude. For control and identification purpose, it is hence more convenient to take the duty cycle of the PWM signals as the input to the LED model.

In this work, both the temperature model and illuminance model of LEDs are described by state space models, where the duty cycle plays the role of not only the input variable, but also a key factor that determines the model parameters. In what follows, the temperature is denoted by t. Time is represented by τ. Luminous flux and illuminance are respectively denoted as Φ and y. The duty cycle of the dimming control signal is represented by u. Then, the first order state space temperature model of LEDs can be written in the following form.

$$\dot{x}(\tau) = A_u \cdot x(\tau) + B_u \cdot u(\tau), \tag{1a}$$
$$t(\tau) = C_u \cdot x(\tau) + D_u \cdot u(\tau). \tag{1b}$$

Here, $x(\tau)$ is the state variable; and A_u, B_u, C_u, D_u are parameters that depend on the input duty cycle, hence with the subscript "u". The duty cycle $0 \leq u(\tau) \leq 1$. Note that since the duty cycle does not instantaneously influence the temperature of the LEDs, the direct feed through term will not be considered in what follows for brevity, i.e. $D_u = 0$.

The total luminous flux emitted from an LED light source at a certain duty cycle decays approximately linearly (with negligible error) with increasing temperature [16], [18], [20], [30]. Let Φ denote the luminous flux, and Φ_0 denote the flux when $u(\tau) = 1$ at the temperature $t = 0^oC$. The luminous flux with an arbitrary duty cycle u and at an arbitrary temperature t can be written as

$$\Phi(u, t) = (\Phi_0 + \rho \cdot t) \cdot u, \tag{2}$$

where $\rho < 0$ is the constant decaying rate of the luminous flux, as t increases.

However, luminous flux is usually measured by an integrating sphere. For real time control of practical lighting systems, it is the illuminance, i.e. the luminous flux per unit area, that is measured by a photosensor. In lighting systems, when the relative positions of a lamp and a photosensor are fixed, the illuminance is proportional to the total luminous flux of the lamp [32]. Hence, the decaying illuminance with increasing temperature t can also be expressed by a linear equation, i.e.

$$y(u, t) = (y_0 + \eta \cdot t) \cdot u, \tag{3}$$

where y_0 is the illuminance with $u(\tau) = 1$ at the temperature $t = 0^oC$; and η is the constant decaying rate.

Substituting the temperature t defined by the dynamic model (1b) into Eq. (3), the dynamic response of the illuminance to the input duty cycle and the temperature can be written as

$$y(\tau) = [y_0 + \eta C_u \cdot x(\tau)] \cdot u(\tau). \tag{4}$$

On the other hand, ambient light also has to be taken into account. We shall refer to the ambient light as the disturbance to the system, and denote it by w in what follows. Incorporating the disturbance w into (4), the state-space model

describing the response of the illuminance to the duty cycle and ambient light shall take the following form.

$$\dot{x}(\tau) = A_u \cdot x(\tau) + B_u \cdot u(\tau), \tag{5a}$$
$$y(\tau) = [y_0 + \eta C_u \cdot x(\tau)] \cdot u(\tau) + w(\tau). \tag{5b}$$

The dynamics is obviously nonlinear.

B. Formulation of the Problems

With the nonlinear dynamics described, we are now ready to state the two main problems to be solved in this work.

Problem 1: Given a set of measured temperature data and their corresponding input duty cycles, identify a dynamic thermal model in the state-space form of (1).

Problem 2: Given a dynamic model in the state-space form of (5), design a controller which tracks the reference illuminance, and is robust to the ambient light disturbance w.

The block diagram of the control loop is shown in Fig. 1.

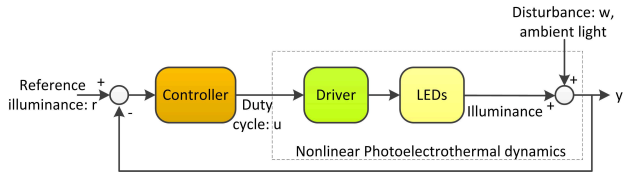

Fig. 1. The feedback control loop for tracking the reference illuminance.

III. System Identification of the Nonlinear Photoelectrothermal Dynamics

This section will solve Problem 1, and identify the nonlinear thermal dynamic model of (1).

A. LPV model description

The state space model (1) contains the parameters that depends on the input duty cycles, i.e. A_u, B_u and C_u; and is hence nonlinear. In this section, the nonlinearity will be described by the following linear parameter varying (LPV) model, whose parameters depend on scheduling parameters.

$$\dot{x}(\tau) = \sum_{i=1}^{n_\mu} \mu_i(\tau) A_i \cdot x(\tau) + \sum_{i=1}^{n_\mu} \mu_i(\tau) B_i \cdot u(\tau), \tag{6a}$$
$$t(\tau) = \sum_{i=1}^{n_\mu} \mu_i(\tau) C_i \cdot x(\tau). \tag{6b}$$

Here, the weights $\mu_i(\tau)$, $i = 1, \cdots, n_\mu$, are real numbers, and depend on the scheduling parameters to be defined later. $\{A_i, B_i, C_i\}$, $i = 1, \cdots, n_\mu$, are a set of model parameters to be identified from experimental data. n_μ is the number of these parameters. For instance, the input dependent state matrix A_u can be written as, $A_u = \sum_{i=1}^{n_\mu} \mu_i(\tau) A_i$.

The scheduling parameters that determine the weights may be the states, the inputs, and/or the outputs, and are measurable. These parameters may have multiple dimensions, and are denoted by $\theta_j, j = 1, \cdots, n_\theta$. In [22], [23], the weights $\mu_i(\tau)$, $i = 1, \cdots, n_\mu$ are defined as the monomials of the scheduling parameters, i.e.

$$\mu_i(\tau) = \theta_1^{\kappa_{i,1}}(\tau) \cdot \theta_2^{\kappa_{i,2}}(\tau) \cdots \theta_{n_\theta}^{\kappa_{i,n_\theta}}(\tau),$$

where $\kappa_{i,j}$ is a natural number; and $0 \leq \sum_{j=1}^{n_\theta} \kappa_{i,j} \leq N$ with N representing the polynomial degree.

For a set of fixed scheduling parameters at an arbitrary time instant, at a fixed working condition, the model (6) is linear time invariant (LTI), and can be identified by any classical system identification techniques [33]. This LTI model is called a local model. When a number of different sets of scheduling parameters and their corresponding local models are available, the unknown parametric matrices, $\{A_i, B_i, C_i\}$, can be estimated by fitting an interpolation function.

Specifically in the LED thermal dynamics, since the parametric matrices of the model (1) depend on the input duty cycles, it is natural to take u as a scheduling parameter. Besides, in lighting applications, the dimming commands are manually input via a control terminal. The changes in dimming level hence cause the duty cycle to change in a stepwise fashion. This motivates to use the change between the two adjacent different duty cycles as another scheduling parameter. In summary, we consider two scheduling parameters that are related to the duty cycles, i.e.

$$\begin{cases} \theta_1(\tau) = & u_p(\tau), \\ \theta_2(\tau) = & u(\tau) - u_p(\tau). \end{cases} \tag{7}$$

Here, $u_p(\tau)$ represents the duty cycle in the nearest past time when the duty cycle is different from the current one. In other words, $u_p(\tau) = u(\tau_p)$ for the largest τ_p, satisfying $\tau_p < \tau$ and $u(\tau_p) \neq u(\tau)$. For brevity, we shall refer to $\theta_1(\tau)$ as the previous duty cycle, and $\theta_2(\tau)$ as the changed duty cycle. Obviously, $0 \leq \theta_1 \leq 1$, $-1 \leq \theta_2 \leq 1$ and $0 \leq \theta_1 + \theta_2 \leq 1$.

The benefit of using two scheduling parameters, instead of just the duty cycle, is that the step size of each dimming action is also taken into account, and can hence better track the transient response, when the duty cycle changes.

The key in LPV identification techniques is to properly find a set of fixed local conditions, which cover the full working range [26]. The local conditions are usually found on a grid of the scheduling parameters [22], [26]. For the two scheduling parameters of the LED thermal dynamics defined in Eq. (7), a step size of 0.2 is taken for both θ_1 and θ_2. There are hence totally 15 local models, corresponding to the following local conditions, i.e. LM1: $\{\theta_1 = 0, \theta_2 = 0.2\}$, LM2: $\{\theta_1 = 0, \theta_2 = 0.4\}$, LM3: $\{\theta_1 = 0, \theta_2 = 0.6\}$, LM4: $\{\theta_1 = 0, \theta_2 = 0.8\}$, LM5: $\{\theta_1 = 0, \theta_2 = 1\}$, LM6: $\{\theta_1 = 0.2, \theta_2 = 0.2\}$, LM7: $\{\theta_1 = 0.2, \theta_2 = 0.4\}$, LM8: $\{\theta_1 = 0.2, \theta_2 = 0.6\}$, LM9: $\{\theta_1 = 0.2, \theta_2 = 0.8\}$, LM10: $\{\theta_1 = 0.4, \theta_2 = 0.2\}$, LM11: $\{\theta_1 = 0.4, \theta_2 = 0.4\}$, LM12: $\{\theta_1 = 0.4, \theta_2 = 0.6\}$, LM13: $\{\theta_1 = 0.6, \theta_2 = 0.2\}$, LM14: $\{\theta_1 = 0.6, \theta_2 = 0.4\}$, LM15: $\{\theta_1 = 0.8, \theta_2 = 0.2\}$.

For the weights defined in Eq. (7), up to the fifth order monomials are tried. The following monomials are found to be the best bases to form the polynomial interpolation function in terms of the fitting accuracy, i.e. $1, \theta_1, \theta_2, \theta_1\theta_2, \theta_1^2, \theta_2^2, \theta_1^2\theta_2, \theta_1^3, \theta_2^3$. So $n_\mu = 9$; and there are 15 local models with 15 different pairs of poles and gains.

B. Identifying a set of LTI local models

To identify an LTI system, a wide range of classical methods can be used. We choose to use the ARX (autoregressive with exogenous inputs) method [33], because it turns out to be superior to the other classical methods in this specific problem of identifying local LED thermal models.

The excitation signals are chosen to be a pseudo-random binary sequence (PRBS), shifting values between θ_1 and $\theta_1 + \theta_2$. Therefore, both dimming up and dimming down are described by the same local model. The rising temperature as dimming up can be followed by the increase in the input duty cycle u; while the descending temperature as dimming down can be tracked by the decrease in it.

The identified first order local models can be realized in the following state-space form.

$$\dot{x}(\tau) = A_j \cdot x(\tau) + u(\tau), \tag{8a}$$
$$t(\tau) = K_j \cdot x(\tau). \tag{8b}$$

Here, A_j, K_j are respectively the pole and gain of the j-th local model. This model is equivalent to the transfer function, $\frac{K_j}{s-A_j}$.

C. Interpolation of the local models

Based on the local models (8), the LPV model (6) of the LED thermal dynamics shall take the following form.

$$\dot{x}(\tau) = \sum_{i=1}^{n_\mu} \mu_i(\tau) A_i \cdot x(\tau) + u(\tau), \tag{9a}$$
$$t(\tau) = \sum_{i=1}^{n_\mu} \mu_i(\tau) K_i \cdot x(\tau). \tag{9b}$$

For brevity, we shall still denote $A_u = \sum_{i=1}^{n_\mu} \mu_i(\tau) A_i$ and $C_u = \sum_{i=1}^{n_\mu} \mu_i(\tau) K_i$, in what follows.

Denote the identified pole and gain of the j-th local model respectively by $\hat{A}_j$ and $\hat{K}_j$, $j = 1, \cdots, M$, where M denotes the number of different local models. The unknown parameters, $A_i, K_i, i = 1, \cdots, n_\mu$, can be estimated by solving the following least squares problem [22].

$$\min_{A_i, K_i, i=1,\cdots,n_\mu} \sum_{j=1}^{M} \left[\left(\hat{A}_j - \sum_{i=1}^{n_\mu} \mu_{i,j} A_i \right)^2 + \left(\hat{K}_j - \sum_{i=1}^{n_\mu} \mu_{i,j} K_i \right)^2 \right], \tag{10}$$

Here, $\mu_{i,j}$ is the i-th weight evaluated at the j-th local condition. Specifically in the LED thermal dynamics, $M = 15, n_\mu = 9$; and $\mu_{i,j}$ are calculated by

$$\mu_{1,j} = 1, \mu_{2,j} = \theta_{1,j}, \mu_{3,j} = \theta_{2,j}, \mu_{4,j} = \theta_{1,j}\theta_{2,j}, \mu_{5,j} = \theta_{1,j}^2,$$
$$\mu_{6,j} = \theta_{2,j}^2, \mu_{7,j} = \theta_{1,j}^2\theta_{2,j}, \mu_{8,j} = \theta_{1,j}^3, \mu_{9,j} = \theta_{2,j}^3,$$

with $\theta_{1,j}, \theta_{2,j}$ representing the two scheduling parameters measured at the j-th local condition.

As a summary, the system identification algorithm of the LPV model (6) take the steps as shown in Fig. 2.

D. Experimental setup

The junction temperature of LEDs is difficult to measure. In [18], an infrared thermal imaging system is used to measure the surface temperature of the LEDs, which is however slightly lower than the junction temperature. In [21], the junction temperature is not directly measured either, but instead estimated by pulse forward voltage method [34]. To avoid the difficulty in measuring the junction temperature, we measure the temperature on the LED board instead. Another benefit of measuring the board temperature is that the heat dissipation of the board is also incorporated in the thermal dynamics, and hence does not have to be modelled alone. Note that the board temperature model depends on several parameters, including the thermal resistance respectively between the junction and the soldering point, between the soldering point and the board, and from the board to the ambient environment. The influence of these parameters is manifested in the measured data, and can in turn be included in the identified model.

The experimental setup is shown in Fig. 3, whose components are listed in Table I. The LEDs are low power with a CCT of 3000K, and are soldered on a MCPCB board. The picture of the LED board and its electrical diagram are shown in Fig. 4. Five strings of three serially connected LEDs are connected in parallel. The LED board is powered by a constant current driver, supplying a $380mA$ current to the entire board. The voltage dropped across each string of serially connected LEDs is $8.9V$. In average, the amplitude of the PWM current signal input to each LED is $76mA$. The fundamental frequency of the PWM signal is set at 1000Hz to avoid flicking. The voltage dropped across each LED is about $2.97V$. Both the current and voltage are within the rated operating range of this type of LED.

The dim port of the driver is connected to an MCU, which

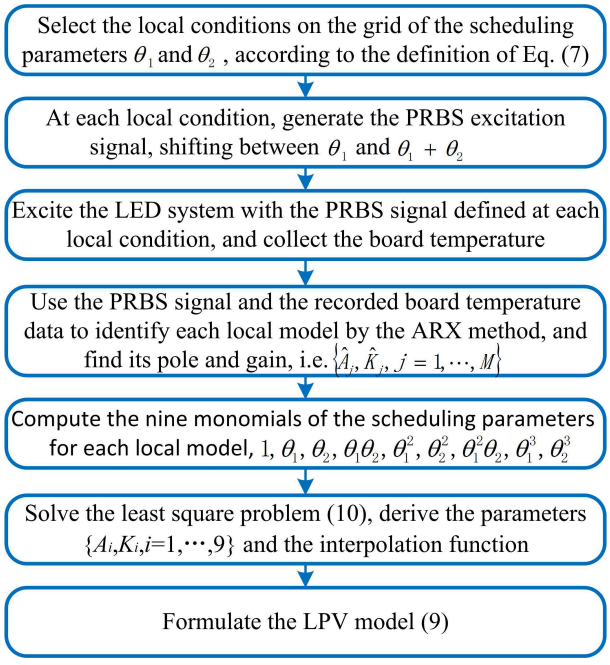

Fig. 2. LPV system identification algorithm for LED systems.

converts the duty cycles to PWM signals. The temperature is measured by a thermal couple glued at the center of the LED board. Another thermal couple is attached in its neighborhood, measuring the ambient temperature. The illuminance from the LEDs is measured by a photodiode. The LED board and the photodiode are mounted in an opaque chamber. The distance between them is 0.8 meters.

In the identification experiments, 15 different PRBS signals, corresponding to the 15 different local conditions, are used to excite the LED thermal dynamics. Each PRBS sequence contains 3600 duty cycles, running for 3600 seconds. The experiment is repeated at each local condition, in order to collect the data to identify each local LTI model. At the beginning of each experiment, the temperature of both the LED board and the chamber is restored to the indoor temperature. The PC stores the PRBS signals in its memory. The sampling interval is set at one second. At each second, the PC reads a duty cycle, and sends it via a USB port to the MCU. In the meantime, the PC sends a reading request via another USB port to the multimeter to read the output from the two thermal couples. The two temperature values are sent back via the same USB port. These steps are completed in one second within one sampling interval. The measured ambient temperature is only used to track the temperature changes in the environment, and is not used in the system identification.

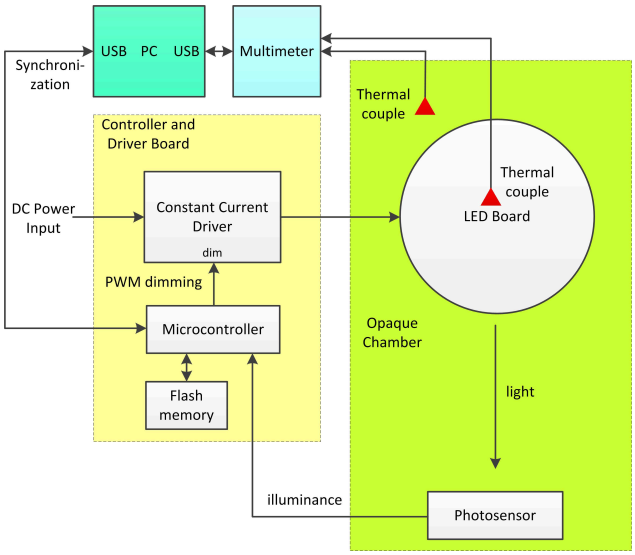

Fig. 3. Experimental setup to measure the temperature response and the illuminance.

E. Identification results

Based on the 15 sets of data measured from the setup, 15 pairs of poles and gains respectively corresponding to the 15 local LTI models are identified. Then, the least squares problem (10) is solved using the identified poles, gains and the corresponding weights. The fitted poles and gains of the 15 local models by the interpolation function are respectively shown in Figs. 5 and 6. The root mean square (RMS) error of the interpolated poles and gains are respectively 1.41×10^{-4} and 8.05×10^{-3}, both less than 5% of their average values.

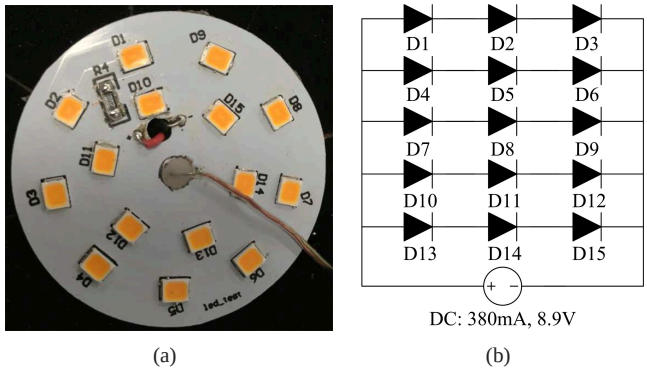

Fig. 4. The LED board used in the experiments. (a) Photo. (b) Electrical diagram.

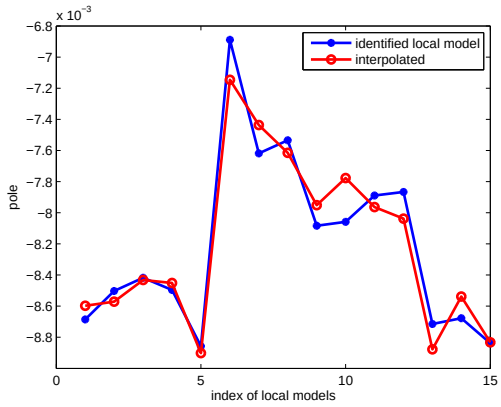

Fig. 5. Fitted poles by the interpolated polynomial function. Dots: poles of the identified local models. Circles: interpolated poles.

The interpolated poles and gains as the functions of the two scheduling parameters, i.e. the previous duty cycle and changed duty cycle, are further illustrated in Figs. 7 and 8. Clearly, both the poles and gains are nonlinear functions of the two scheduling parameters. Moreover, it can be seen from Fig. 7 that the fastest pole appears when $\theta_1 = 0$ and $\theta_2 = 0.8$;

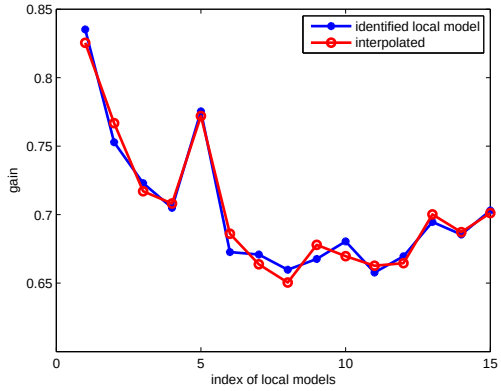

Fig. 6. Fitted gains by the interpolated polynomial function. Dots: poles of the identified local models. Circles: interpolated poles.

TABLE I
COMPONENTS OF THE EXPERIMENTAL SETUP

Type	Name	Parameters
LED	Everlight 67-21S/KK2C-H3030M31N42936Z6/2T	CCT: 3000K, forward current: $75 \sim 100mA$, forward voltage: $2.9 \sim 3.6V$
Multimeter	Keithley 2700 and Keithley 7700 multiplexer	temperature range: $-200 \sim 1820^oC$
Thermal couple	OMEGA K-SM-TT-36-36	range: $-200 \sim 1372^oC$, precision: 0.001^oC
MCU	STM32F030C8T6	48MHz frequency, 64KB flash memory
Photodiode	Hamamatsu S7686	response time: 0.5 microseconds

while the slowest appears when $\theta_1 = 0$ and $\theta_2 = 0.2$. Besides, larger step changes in the duty cycle generally yield faster poles. On the other hand, it can be seen from Fig. 8 that the largest gain appears when $\theta_1, \theta_2 < 0.1$; while the smallest appears when $\theta_1 + \theta_2 \approx 1$.

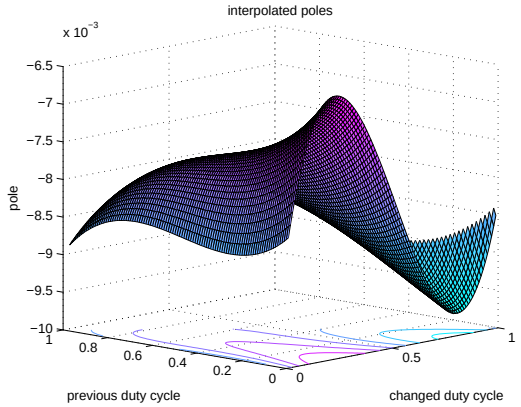

Fig. 7. Interpolated poles as the function of the previous duty cycles and the changed duty cycles.

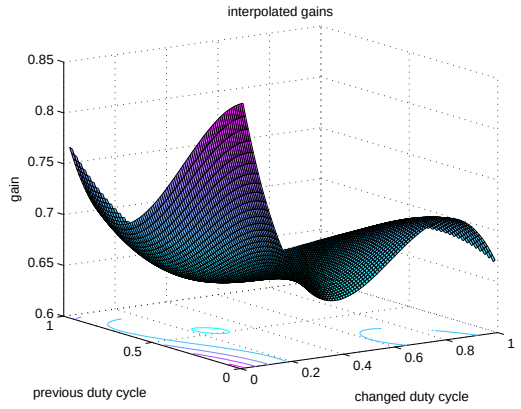

Fig. 8. Interpolated gains as the function of the previous duty cycles and the changed duty cycles.

The identified LPV model is verified in an experiment with the duty cycles continuously changing from 0 to 0.1, from 0.1 to 0.3, from 0.3 to 0.5, from 0.5 to 0.7, from 0.7 to 0.9, from 0.9 to 0.7, from 0.7 to 0.5, and finally from 0.5 to 1. The total time spent in the experiment is 2700 seconds. The board temperature is recorded every one second. Three different models are compared in terms of the fitting errors, i.e. the identified LPV model, the average of the 15 local models and the identified local LTI model at the local condition $\theta_1 = 0, \theta_2 = 1$, i.e. LM5. The fitting errors are respectively 1.83^oC by the identified LPV model, 3.16^oC by the average LTI model, and 4.38^oC by the identified local LTI model. Clearly, the identified LPV model outperforms the other two LTI models in terms of the fitting accuracy.

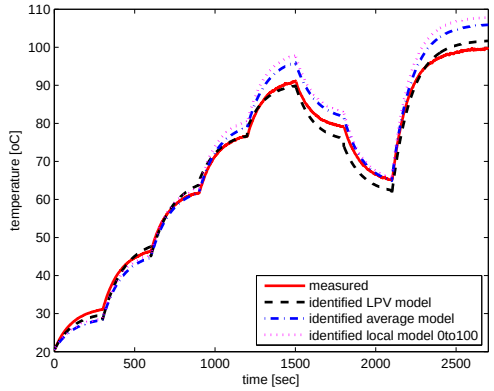

Fig. 9. Simulated board temperature by the identified LPV model, compared with the measured and the simulated board temperatures by the average model and the local model at $\theta_1 = 0, \theta_2 = 1$.

IV. $\mathcal{H}_\infty$ CONTROL ROBUST TO THERMAL EFFICACY DEGRADATION AND AMBIENT LIGHT

Based on the identified thermal model (1), Problem 2 will be solved in this section.

A. The illuminance model

As described in Sec. II, the illuminance measured by a photosensor can be calculated by Eq. (3). When the relative position of the photosensor and the LED light source is fixed, the two parameters, y_0 and η in (3) are constant, and can be estimated from the experimental data. The experiment is conducted as follows. First, an integrating sphere is used to measure the total luminous flux as the temperature rises. The duty cycle is fixed at 1. The temperature is controlled by the heater mounted beneath the LED board, and measured by the thermal couple glued on it. The two parameters in (2) are respectively found to be $\Phi_0 = 590.16lm$ and $\rho = -0.9614lm/^oC$, which accurately fit the measured data in a linear fashion. Then, the linear relation between the total luminous flux and the measured illuminance is estimated using the data collected from the setup shown in Fig. 3. In this experiment, the duty cycle is gradually increased from

0 to 1 with a step size of 0.1. The board temperature and the illuminance are recorded at each duty cycle. The flux at each duty cycle is calculated by (2). Fitting by least squares results in $y = 10.1891 + 0.3226 \cdot \Phi$. Combining the two linear equations, the fitted equation of (3) can be written as $y(u,t) = (200.5795 - 0.3101 \cdot t) \cdot u$.

Recall that the illuminance equation in (5b) is in a nonlinear form. But it can be further developed into a linear parameter varying form by absorbing the input duty cycle into the parametric matrices, i.e.

$$y(\tau) = [\eta C_u u(\tau)] \cdot x(\tau) + y_0 \cdot u(\tau) + w(\tau). \quad (11)$$

Here, $C_u = \sum_{i=1}^{n_\mu} \mu_i(\tau) K_i$. Note that in this way, the nonlinear state-space model (5) is changed to the LPV model of (5a,11).

On the other hand, we consider trajectory tracking problem, instead of stabilizing control. Therefore, we need to derive the tracking error dynamics. Denote the reference illuminance by $r(\tau)$. The tracking error is $e(\tau) = r(\tau) - y(\tau)$. Substituting the illuminance $y(\tau)$ in (11) into this expression, $e(\tau)$ then takes the following form.

$$e(\tau) = (-\eta C_u u) \cdot x(\tau) + (-y_0) \cdot u(\tau) + r(\tau) - w(\tau). \quad (12)$$

The goal of the trajectory tracking control is to guarantee that the error dynamics defined by the system (5a,12) is asymptotically stable, i.e. $\lim_{\tau\to\infty} e(\tau) = 0$. To this end, we include an integral action into the system (5a,12), because the integral control is able to yield zero tracking error at steady state. The integrator can be realized as follows.

$$\dot{x}_2(\tau) = (-\eta C_u u)x(\tau) + (-y_0)u(\tau) + r(\tau) - w(\tau), \quad (13a)$$
$$e_2(\tau) = x_2(\tau). \quad (13b)$$

Now, combing (5a), (12) and (13), and taking the reference and the illuminance from the ambient light into a new disturbance vector, the error dynamics can be written as

$$\begin{bmatrix} \dot{x}_1 \\ \dot{x}_2 \end{bmatrix} = \begin{bmatrix} A_u & 0 \\ -\eta C_u u & 0 \end{bmatrix} \begin{bmatrix} x_1 \\ x_2 \end{bmatrix} + \begin{bmatrix} 1 \\ -y_0 \end{bmatrix} u + \begin{bmatrix} 0 & 0 \\ 1 & -1 \end{bmatrix} \begin{bmatrix} r \\ w \end{bmatrix}, \quad (14a)$$

$$\begin{bmatrix} e_1 \\ e_2 \end{bmatrix} = \begin{bmatrix} -\eta C_u u & 0 \\ 0 & 1 \end{bmatrix} \begin{bmatrix} x_1 \\ x_2 \end{bmatrix} + \begin{bmatrix} -y_0 \\ 0 \end{bmatrix} u + \begin{bmatrix} 1 & -1 \\ 0 & 0 \end{bmatrix} \begin{bmatrix} r \\ w \end{bmatrix}, \quad (14b)$$

$$z = \begin{bmatrix} 0 & 1 \end{bmatrix} \begin{bmatrix} x_1 \\ x_2 \end{bmatrix} + 0 \cdot u + \begin{bmatrix} 0 & 0 \end{bmatrix} \begin{bmatrix} r \\ w \end{bmatrix}. \quad (14c)$$

Here, e_1 is the instant tracking error; while e_2 is the integrated tracking error over time. $z = e_2$ is the controlled output to be used in the $\mathcal{H}_\infty$ control method to be introduced next.

B. LPV $\mathcal{H}_\infty$ control method

Since the system (9) is first order and stable at each individual local condition, a PID controller suffices to yield an acceptable tracking performance. Moreover, since both the ambient light and the reference illuminance appear as the disturbance to the LPV system (14), another objective of the control is to ensure the robust tracking performance subject to these disturbances. The robust PID control synthesis methods proposed in [35] can realize these objectives.

Denote the parametric matrices in (14) as follows.

$$A_\mu = \begin{bmatrix} A_u & 0 \\ -\eta C_u u & 0 \end{bmatrix}, B_\mu = \begin{bmatrix} 1 \\ -y_0 \end{bmatrix}, E_\mu = \begin{bmatrix} 0 & 0 \\ 1 & -1 \end{bmatrix},$$
$$C_\mu^y = \begin{bmatrix} -\eta C_u u & 0 \\ 0 & 1 \end{bmatrix}, D_\mu^y = \begin{bmatrix} -y_0 \\ 0 \end{bmatrix}, E_\mu^y = \begin{bmatrix} 1 & -1 \\ 0 & 0 \end{bmatrix},$$
$$C_\mu^z = \begin{bmatrix} 0 & 1 \end{bmatrix}, D_\mu^z = 0, E_\mu^z = \begin{bmatrix} 0 & 0 \end{bmatrix}.$$

Denote $x = [x_1\ x_2]^T$, $e = [e_1\ e_2]^T$ and the disturbance vector by $d = [r\ w]^T$, where the superscript "T" denotes matrix transpose. Then, the LPV model (14) can be simplified to

$$\dot{x} = A_\mu x + B_\mu u + E_\mu d, \quad (15a)$$
$$e = C_\mu^y x + D_\mu^y u + F_\mu^y d, \quad (15b)$$
$$z = C_\mu^z x + D_\mu^z u + F_\mu^z d. \quad (15c)$$

The parametric matrices are continuous matrix valued functions of the weights $\mu \in \Omega \subset \mathbb{R}^{n_\mu}$,[1] with Ω being a compact hyper rectangle. The robust control problem is to design a controller for the system (15) to guarantee the closed loop stability and that the $\mathcal{H}_\infty$ norm, defined by $\max_{d\neq 0} \frac{\|z\|_2}{\|d\|_2}$, is bounded.

Since D_μ^z is null $\forall \mu \in \Omega$; and B_μ is a parameter independent full column rank matrix, a numerically tractable solution of this problem is to design a PI controller by solving linear matrix inequalities (LMIs) [35].

On the other hand, since integral action is included in the system (14), one only needs to design a proportional controller using the two error signals, e_1, e_2. We shall rewrite Corollary 6 in [35] specifically for the system (14) in the following lemma.

Lemma 1: System (14) is quadratically stabilizable with a given rate of convergence $\beta > 0$ and an $\mathcal{H}_\infty$ norm bound less than a positive number γ, if there exist two positive numbers $\mathcal{P}_1$ and $\mathcal{P}_2$ and a given matrix $W_y \in \mathbb{R}^{1\times 2}$, such that the LMIs defined in (16) holds.[2] In (16), $\mathcal{P} = \begin{bmatrix} \mathcal{P}_1 & \\ & \mathcal{P}_2 \end{bmatrix}$; $\tilde{A}_\mu = V^{-1}[A_\mu + \beta I]V$, $\tilde{E}_\mu = V^{-1}E_\mu$, $\tilde{C}_\mu^y = C_\mu^y V$, $\tilde{C}_\mu^z = C_\mu^z V$, with V denoting a nonsingular transformation matrix such that $V^{-1}B_\mu = [1\ 0]^T$. In this case, a possible value for the output feedback matrix gain is $G = \mathcal{P}_1^{-1} W_y \in \mathbb{R}^{1\times 2}$. □

Note that the LMIs (16) only need to be evaluated at all the vertices of the hyper rectangle Ω. The feedback gain $G \in \mathbb{R}^{1\times 2}$ only contains the proportional part. Denote the proportional gain by $K_p \in \mathbb{R}^{1\times 2}$, which can be derived as $K_p = G\left(I + D_\mu^y G\right)^{-1}$. Then, the control input can be calculated by

$$u(\tau) = K_p^T \cdot \begin{bmatrix} e_1(\tau) \\ e_2(\tau) \end{bmatrix}.$$

The first element in K_p hence corresponds to the proportional gain, and the second element corresponds to the integral gain.

It is also straightforward to derive a pure integral controller by only considering the integral error in (14b), i.e.

$$e = \begin{bmatrix} 0 & 1 \end{bmatrix} \cdot \begin{bmatrix} x_1 \\ x_2 \end{bmatrix} + 0 \cdot u + \begin{bmatrix} 0 & 0 \end{bmatrix} \cdot \begin{bmatrix} r \\ w \end{bmatrix}.$$

[1]The set of real n-dimensional vectors and the set of real matrices with n rows and m columns are respectively denoted by $\mathbb{R}^n$ and $\mathbb{R}^{n\times m}$.

[2]A matrix $\mathcal{M}$ is negative definite, if $\mathcal{M} \prec 0$. The symbol "I" denotes an identity matrix with proper dimensions.

$$\begin{bmatrix} \tilde{A}_\mu^T\mathcal{P}+\mathcal{P}\tilde{A}_\mu+\begin{bmatrix} W_y \\ 0 \end{bmatrix}\tilde{C}_\mu^y+(\tilde{C}_\mu^y)^T\begin{bmatrix} W_y \\ 0 \end{bmatrix}^T & \mathcal{P}\tilde{E}_\mu+\begin{bmatrix} W_y \\ 0 \end{bmatrix}F_\mu^y & \gamma^{-1}(\tilde{C}_\mu^z)^T \\ E_\mu^T\mathcal{P}+(F_\mu^y)^T\begin{bmatrix} W_y \\ 0 \end{bmatrix}^T & -I & \gamma^{-1}(F_\mu^z)^T \\ \gamma^{-1}\tilde{C}_\mu^z & \gamma^{-1}F_\mu^z & -I \end{bmatrix} \prec 0,\ \forall\mu\in\Omega. \tag{16}$$

C. Robust tracking controller design

In (14), A_u and C_u can be interpolated by the LPV model (6). However, the dependence of $C_u u$ on the two scheduling parameters is more complicated. To see this, note that $C_u u = \sum_{i=1}^{n_\mu}\mu_i(\tau)C_i\cdot(\theta_1+\theta_2)$, where $n_\mu = 9$.

The new monomials include $\theta_1, \theta_2, \theta_1\theta_2, \theta_1^2, \theta_2^2, \theta_1^2\theta_2, \theta_1\theta_2^2, \theta_1^3, \theta_2^3, \theta_1^3\theta_2, \theta_1\theta_2^3, \theta_1^2\theta_2^2, \theta_1^4, \theta_2^4$. The number of weights is $n'_\mu = 14$. The LMIs (16) need to be evaluated at all the 2^{14} vertices of the hyper rectangle Ω. The vertices contain all the possible combinations of the min or max value of each monomial evaluated on $0 \le \theta_1, \theta_2 \le 1$. Though the number of the vertices is large, these LMIs can be solved within one minute by the LMI solver of MATLAB on a PC with a 2.6GHz CPU.

Both the PI and pure integral controllers are designed and tested in the experiments. It is found that the PI controller results in severe oscillations in the closed loop response of the illuminance; while the pure integral controller leads to very fast convergence to the reference illuminance and no flickering at all. The integral gain is found to be $K_I = 0.165387$.

Note that the designed controller is in continuous time. It needs to be discretized to be implemented on an MCU. To ensure a fast convergence, the sampling interval for the controller is set as 0.01 seconds. The integral controller, $u(\tau) = K_I\cdot\int_0^\tau[r(\varphi)-y(\varphi)]d\varphi$, is hence changed to

$$u(k) = 0.01\cdot K_I\cdot\sum_{i=1}^{k}[r(i)-y(i)]. \tag{17}$$

D. Closed-loop experiments

In the closed-loop experiments, the integral controller (17) is implemented on the MCU. The MCU samples the photodiode at a rate of 100Hz. The calculated duty cycles and the measured illuminance are streamed to the memory of the PC via a serial port of the MCU and a USB port of the PC. The board temperature is also measured simultaneously, but at a rate of 1Hz, to record the temperature variation. Four experiments have been performed as follows.

The first experiment is to track a constant illuminance of 200lux with the illuminance from the ambient light set at 50lux. The ambient light is generated by another LED board of the same type as the one shown in Fig. 4. This light source is mounted beside the controlled LED board in the opaque chamber. The experiment lasts for 1200 seconds. The closed loop response is shown in Fig. 10. Clearly, the illuminance reaches the target within the beginning 0.2 seconds. Besides, the controller can keep the illuminance at the target value as the temperature rises and in the presence of the ambient light.

The board and the ambient temperature are respectively 69^oC and 24.6^oC at the end of this experiment. From the datasheet of the LED, the thermal resistance between the junction and the soldering point is $50^oC/W$. The thermal resistance respectively between the soldering point and the board and from the board to the ambient environment are estimated to be $2^oC/W$ and $12^oC/W$. Based on the steady-state temperature equation in [30], the junction temperature of the LEDs is estimated to be 75.1^oC, much lower than its rated max value, 125^oC. On the other hand, the duty cycle increases from 0.6 to 0.65. But since the LEDs are driven by a constant current source, the amplitude of the PWM current waveform to each LED is maintained around $76mA$. Therefore, both the temperature and the current are controlled within the rated operating range of this type of LEDs.

The second experiment is to track a constant illuminance of 180lux, but with varying illuminance levels from the ambient light. At the beginning, the ambient illuminance is 0. Around the 200th second, it is increased to 30lux; and then changed to 25lux at the 400th second and to 40lux at the 600th second. The ambient illuminance becomes 60lux around the 800th second, and holds unchanged until the end of the experiment. This experiment also lasts for 1200 seconds. The closed loop response is shown in Fig. 11. Clearly, the measured illuminance jumps at each time when the ambient illuminance changes, but quickly gets back to the target value again within 0.1 seconds. The slight fluctuations in the duty cycle is due to the fact that the ambient illumination is not controlled in closed loop, but only driven by a constant current source. Therefore, the ambient illumination may fluctuate as the temperature changes and due to the small ripples in the driving current. The descending trend of the temperature is due to the increases in the ambient illuminance, and hence the decreases of the duty cycles to the controlled LED board.

The third experiment is to track varying illuminance references without ambient light. The reference trajectory and the measured illuminance in the closed loop are shown in Fig. 12. Clearly, both the step changes and the continuous changes in the reference illuminance can be tracked by the controller.

In the last experiment, a new LED board with 12 LEDs of the same type is tested in closed loop. Unlike the LED board used in the first three tests, this new board contains four parallel connected LED strings. Each string also contains three serially connected LEDs. The amplitude of the forward current to the entire board is $304mA$, and the voltage drop across it is $8.9V$. The amplitude of the current to each LED is also $76mA$. The same control law as in the first three tests is used to track the varying illuminance references as in the third test, without ambient light. The reference trajectory and the measured illuminance in the closed loop are shown in Fig. 13. Clearly, the control law is also effective in controlling the light source with different number of LEDs of the same type.

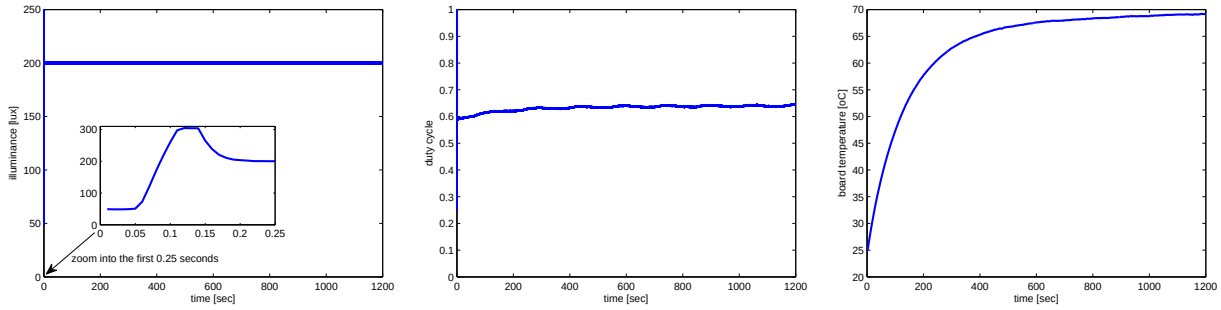

(a) (b) (c)

Fig. 10. Closed loop response when tracking the constant illuminance of 200lux with constant ambient illuminance of 50lux. (a) Measured illuminance. (b) Duty cycles. (c) Measured temperature.

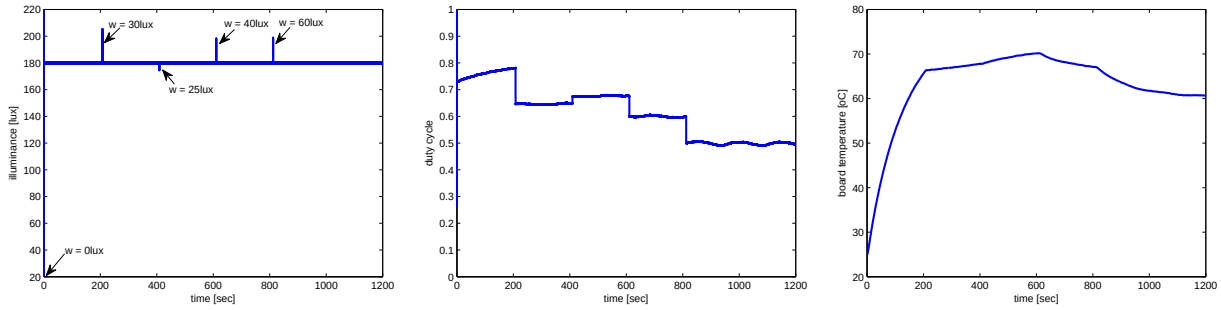

(a) (b) (c)

Fig. 11. Closed loop response when tracking the constant illuminance of 150lux with changing ambient illuminance. (a) Measured illuminance. (b) Duty cycles. (c) Measured temperature.

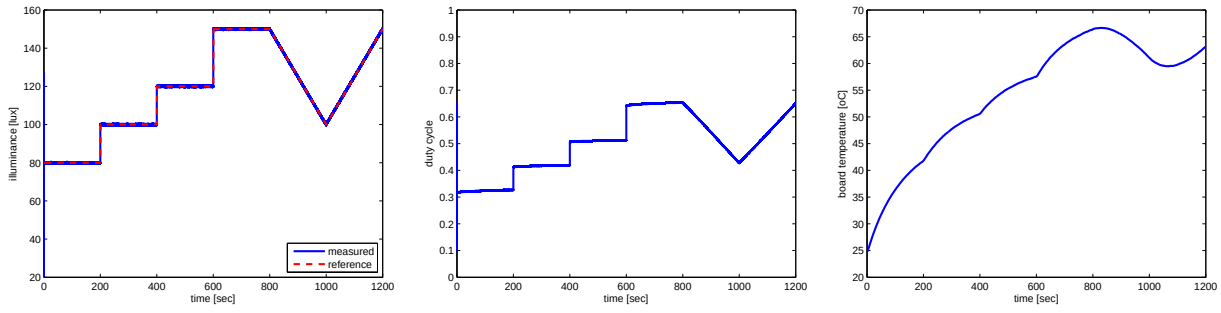

(a) (b) (c)

Fig. 12. Closed loop response when tracking the varying illuminance without ambient light. (a) Measured illuminance. (b) Duty cycles. (c) Measured temperature.

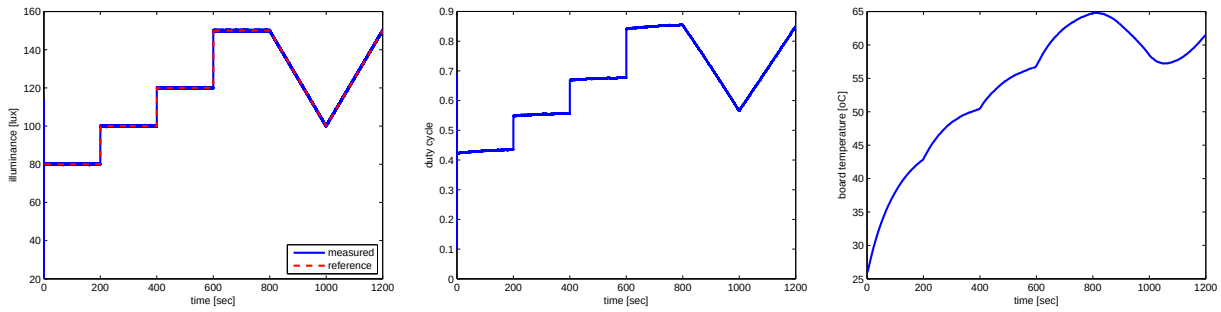

(a) (b) (c)

Fig. 13. Closed loop response of a new LED board with 12 LEDs of the same type to varying reference illuminance without ambient light. (a) Measured illuminance. (b) Duty cycles. (c) Measured temperature.

V. Conclusions

In this paper, we have investigated the methods of identifying the nonlinear thermal dynamics of LED systems by interpolation based LPV identification techniques. The identified LPV model is verified in experiments to have higher fitting accuracy than the identified LTI models at either a single working condition or by averaging different local models. The nonlinear thermal dynamics is then incorporated with the illuminance model, leading to a nonlinear photoelectrothermal model. To design a controller to track the reference illuminance, while attenuating the disturbance from ambient light, we have applied an $\mathcal{H}_\infty$ LPV controller synthesis method. The closed loop control experiments have confirmed the robust performance of the designed controller to both the ambient light disturbance and the fluctuating temperature.

The novelty of this work is treating the nonlinear PET dynamics of LED systems in the LPV framework. The model identification and the robust control design are both originated from the real life data collected from the experimental setup, and are practical to implement. In fact, theoretical modeling also needs parameters, e.g. thermal resistance and lumen efficacy, which may be available in the LED datasheet. However, since the data from the datasheet are not always complete and accurate, experiments are still needed to fit the parameters. In this work, the dynamic temperature model is identified from measured data, which carry the information of both the dynamics and its parameters. By using this "data driven" method, the two steps of theoretical modelling and finding the model parameters are reduced into only one step. On the other hand, the controller designed by the $\mathcal{H}_\infty$ LPV control technique only contains constant gains, and can be easily implemented on a low-end MCU in an LED lamp.

The potential extensions of the current work include controlling the light chromaticity of polychromatic LED systems with the robustness to temperature changes and ambient light disturbance, and developing fault diagnosis methods to monitor the health of LED systems, with the aforementioned robustness.

References

[1] E. Schubert and J. Kim, "Solid-state light sources getting smart," *Science*, vol. 308, no. 5726, pp. 1274–1278, May. 2005.
[2] X. Wu, J. Zhang, and Z. Qian, "Simple two-channel LED driver with automatic precise current sharing," *IEEE Trans. Ind. Electron.*, vol. 58, no. 10, pp. 4783–4788, Oct. 2011.
[3] S. Moon, G. Koo, and G. Moon, "Dimming-feedback control method for triac dimmable led drivers," *IEEE Trans. Ind. Electron.*, vol. 62, no. 2, pp. 960–965, Feb. 2015.
[4] Y. Ye, K. Cheng, J. Lin, and D. Wang, "Single-switch multichannel current-balancing LED drive circuits based on optimized SC techniques," *IEEE Trans. Ind. Electron.*, vol. 62, no. 8, pp. 4761–4768, Aug. 2015.
[5] Y. Li, "A novel control scheme of quasi-resonant valley-switching for high-power-factor AC-to-DC LED drivers," *IEEE Trans. Ind. Electron.*, vol. 62, no. 8, pp. 4787–4794, Aug. 2015.
[6] A. Shrivastava, B. Singh, and S. Pal, "A novel wall-switched step-dimming concept in LED lighting systems using PFC zeta converter," *IEEE Trans. Ind. Electron.*, vol. 62, no. 10, pp. 6272–6283, Oct. 2015.
[7] I. Moreno, "Image-like illumination with led arrays: design," *Opt. Lett.*, vol. 37, no. 5, pp. 839–841, Mar. 2012.
[8] I. Moreno and U. Contreras, "Color distribution from multicolor led arrays," *Opt. Express*, vol. 15, no. 6, pp. 3607–3618, Mar. 2007.
[9] A. Pandharipande and D. Caicedo, "Daylight integrated illumination control of LED systems based on enhanced presence sensing," *Energy Build.*, vol. 43, no. 4, pp. 944–950, Apr. 2011.
[10] J. Dong, W. van Driel, and G. Zhang, "Automatic diagnosis and control of distributed solid state lighting systems," *Opt. Express*, vol. 19, no. 7, pp. 5772–5784, Mar. 2011.
[11] J. Dong and A. Pandharipande, "Efficient distributed control of light-emitting diode array lighting systems," *Opt. Lett.*, vol. 37, no. 14, pp. 2910–2912, Jul. 2012.
[12] N. van de Meugheuvel, A. Pandharipande, D. Caicedo, and P. van den Hof, "Distributed lighting control with daylight and occupancy adaptation," *Energy Build.*, vol. 75, pp. 321–329, Jun. 2014.
[13] P. Deurenberg, C. Hoelen, J. van Meurs, and J. Ansems, "Achieving color point stability in RGB multi-chip LED modules using various color control loops," in *Proc. SPIE*, vol. 5941, Jul. 2005, pp. 63–74.
[14] N. Narendran, Y. Gu, J. Freyssinier, H. Yu, and L. Deng, "Solid-state lighting: failure analysis of white LEDs," *J. Cryst. Growth*, vol. 268, no. 3–4, pp. 449–456, Aug. 2004.
[15] J. Fan, K. Yung, and M. Pecht, "Physics-of-failure-based prognostics and health management for high-power white light-emitting diode lighting," *IEEE Trans. Device Mater. Reliab.*, vol. 11, no. 3, pp. 407–416, Sept. 2011.
[16] H. Chen, Y. Cheung, H. Choi, and S. Hui, "Reduction of thermal resistance and optical power loss using thin-film light-emitting diode (LED) structure," *IEEE Trans. Ind. Electron.*, vol. 62, no. 11, pp. 6925–6933, Nov. 2015.
[17] H. Chen and S. Hui, "Dynamic prediction of correlated color temperature and color rendering index of phosphor-coated white light-emitting diodes," *IEEE Trans. Ind. Electron.*, vol. 61, no. 2, pp. 784–797, Feb. 2014.
[18] H. Chen, D. Lin, S. Tan, and S. Hui, "Chromatic, photometric and thermal modeling of LED systems with nonidentical LED devices," *IEEE Trans. Power Electron.*, vol. 29, no. 12, pp. 6636–6647, Dec. 2014.
[19] B. Huang, P. Hsu, M. Wu, and C. Tang, "Study of system dynamics model and control of a high-power LED lighting luminaire," *Energy*, vol. 32, no. 11, pp. 2187–2198, Nov. 2007.
[20] B. Huang and C. Tang, "Thermalelectricalluminous model of multi-chip polychromatic LED luminaire," *Appl. Therm. Eng.*, vol. 29, no. 16, pp. 3366–3373, Nov. 2009.
[21] F. Wang, C. Tang, and B. Huang, "Multivariable robust control for a redgreenblue LED lighting system," *IEEE Trans. Power Electron.*, vol. 25, no. 2, pp. 417–428, Feb. 2010.
[22] J. D. Caigny, J. Camino, and J. Swevers, "Interpolating model identification for SISO linear parameter-varying systems," *Mech. Syst. Sig. Process.*, vol. 23, no. 8, pp. 2395–2417, Nov. 2009.
[23] J. D. Caigny, J. Camino, and J. Swevers, "Interpolation-based modeling of MIMO LPV systems," *IEEE Trans. Control Syst. Technol.*, vol. 19, no. 1, pp. 46–63, Jan. 2011.
[24] V. Laurain, M. Gilson, R. Tóth, and H. Garnier, "Refined instrumental variable methods for identification of LPV box-jenkins models," *Automatica*, vol. 46, no. 6, pp. 959–967, Jun. 2010.
[25] Y. Zhao, B. Huang, H. Su, and J. Chu, "Prediction error method for identification of LPV models," *J. Process Control*, vol. 22, no. 1, pp. 180–193, Jan. 2012.
[26] A. Bachnas, R. Tóth, A. Mesbah, and J. Ludlage, "A review on data-driven linear parameter-varying modeling approaches: A high-purity distillation column case study," *J. Process Control*, vol. 24, no. 4, pp. 272–285, Apr. 2014.
[27] V. Bender, A. Cardoso, G. Flores, C. Rech, and T. Marchesan, "Electrothermal feedback of a LED lighting system: Modeling and control," in *Proc. 38th IEEE IECON*, Oct. 2012, pp. 4545–4550.
[28] M. Roes, J. Duarte, and M. A. M. Hendrix, "Disturbance observer-based control of a dual-output LLC converter for solid-state lighting applications," *IEEE Trans. Power Electron.*, vol. 26, no. 7, pp. 2018–2027, Jul. 2011.
[29] S. Baccari, M. Tipaldi, L. Iannelli, and F. Vasca, "Photoelectrothermal model predictive control for light emitting diodes," in *Proc. 51st IEEE CDC*, Dec. 2012, pp. 394–399.
[30] X. Tao and S. Hui, "Dynamic photoelectrothermal theory for LED systems," *IEEE Trans. Ind. Electron.*, vol. 59, no. 4, pp. 1751–1759, Apr. 2012.
[31] H. Yang, J. Bergmans, and T. Schenk, "Illumination sensing in LED lighting systems based on frequency-division multiplexing," *IEEE Trans. Signal Process.*, vol. 57, no. 11, pp. 4269–4281, Nov. 2009.
[32] A. Lee, H. Chen, S. Tan, H. Choi, and S. Hui, "Precise dimming and color control of LED systems based on color mixing," *IEEE Trans. Power Electron.*, vol. 31, no. 1, pp. 65–80, Jan. 2016.
[33] L. Ljung, *System identification: Theory for the user*. Prentice Hall, 1987.

[34] T. Brückner and S. Bernet, "Estimation and measurement of junction temperatures in a three-level voltage source converter," *IEEE Trans. Power Electron.*, vol. 22, no. 1, pp. 3–12, Jan. 2007.
[35] M. Mattei, "Robust multivariable PID control for linear parameter varying systems," *Automatica*, vol. 37, no. 12, pp. 1997–2003, Dec. 2001.

Jianfei Dong received the M.Eng. degree in mechatronics from the National University of Singapore, Singapore, in 2005, and the Ph.D. degree in systems and control from Delft University of Technology (TUD), the Netherlands, in 2009.

From November 2009 to July 2011, he was a Postdoctoral Researcher at TUD. From September 2011 to August 2012, he was a Research Scientist with Philips Research, Eindhoven, the Netherlands. Then, he was with the state key lab of solid state lighting of China as the Program Director of intelligent lighting control solutions. He is now a Professor with Suzhou Institute of Biomedical Engineering and Technology, Chinese Academy of Sciences, Suzhou, China. Since September 2011, he has also been a Supervisor of Ph.D. candidates with Beijing Research Center of TUD. His current research interests include data driven design methodologies for control and fault diagnosis, statistical signal analysis, artificial intelligence and their applications in optoelectronic and mechatronic systems.

Guoqi Zhang (M'03-F'14) received his Ph.D. degree in aerospace engineering at Delft University of Technology, Delft, the Netherlands, in 1993.

He is currently a Chair Professor in the Department of Microelectronics at Delft University of Technology since 2013. His research focuses on heterogeneous micro/nano-electronics packaging, system integration and reliability. Prof. Zhang had been with Philips for 20 years: Principal Scientist (1994-1996), Technology Domain Manager (1996-2005), Senior Director of Technology Strategy (2005-2009), and the Philips Fellow (2009-2013). From 2002, he also had part-time appointments as Professor at Technical University of Eindhoven (2002-2005), and Chair Professor at Delft University of Technology (2005-2013).

Prof. Zhang is one of pioneers in developing More than Moore (MtM) strategy when he served as Chair of MtM technology team of Europeans Nanoelectronics Platform (ENIAC) in 2005. Prof. Zhang has published more than 350 papers including more than 140 journal papers, 3 books, and 17 book chapters, and more than 100 patents. He was awarded Outstanding Contributions to Reliability Research by European Center for Micro/Nanoreliability, Berlin in 2007. He received Excellent Leadership Award at EuroSimE and Special Achievement Award at ICEPT. He was elected as IEEE Fellow in 2014, and received IEEE CPMT Outstanding Sustained Technical Contribution Award in 2015.